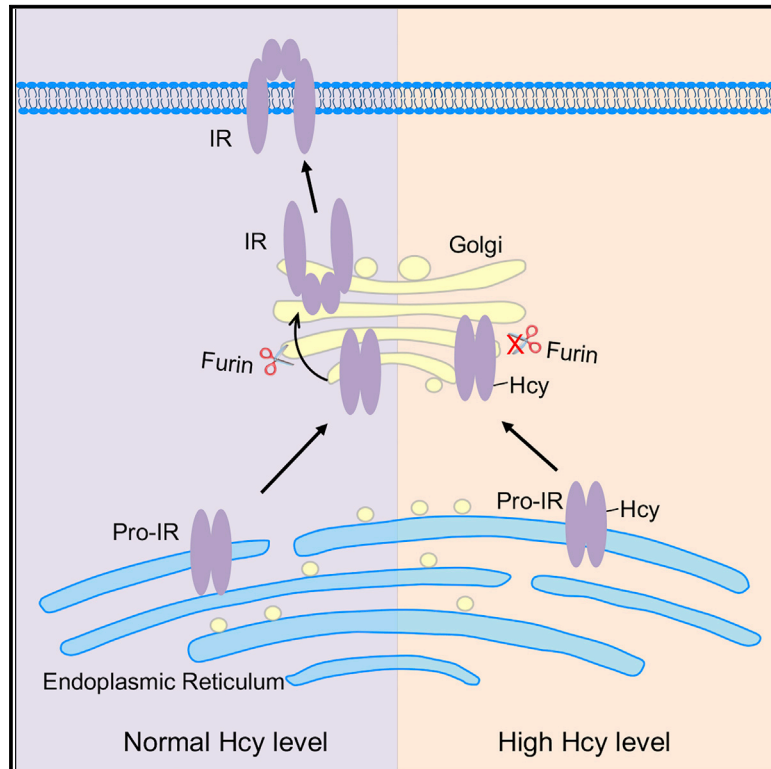# Homocysteine inhibits pro-insulin receptor cleavage and causes insulin resistance via protein cysteine-homocysteinylation

Graphical abstract

Authors

Xuan Zhang, Yuan-Yuan Qu, Lian Liu, ..., Wei Xu, Jing Cao, Jian-Yuan Zhao

Correspondence

zhaojy@fudan.edu.cn

In brief

Zhang et al. show that homocysteine (Hcy) induces insulin resistance and causes diabetic phenotypes by protein cysteine-homocysteinylation of the pro-insulin receptor. The findings suggest that cysteine-homocysteinylation in the endoplasmic reticulum could be an ideal therapeutic target to prevent insulin resistance.

Highlights

- Increased levels of Hcy decrease the abundance of IR-α and IR-β

- Hcy reacts with pro-IR through its thiol group and thus regulates pro-IR cleavage

- Furin plays an important role in cleavage of pro-IR into its mature/active forms

- Inhibition of cysteine-homocysteinylation refreshes the insulin signal

CelPress

Cell Reports

Article

Homocysteine inhibits pro-insulin receptor cleavage and causes insulin resistance via protein cysteine-homocysteinylation

Xuan Zhang,[1] Yuan-Yuan Qu,[1] Lian Liu,[1] Ya-Nan Qiao,[1] Hao-Ran Geng,[1] Yan Lin,[1] Wei Xu,[1] Jing Cao,[2] and Jian-Yuan Zhao[1,2,3,*]

[1]State Key Laboratory of Genetic Engineering, Zhongshan Hospital of Fudan University, School of Life Sciences, Children's Hospital of Fudan University, Fudan University Shanghai Cancer Center, and Institutes of Biomedical Sciences, Fudan University, Shanghai 200438, P.R. China
[2]Department of Anatomy and Neuroscience Research Institute, School of Basic Medical Sciences, Zhengzhou University, Zhengzhou 450001, China
[3]Lead contact
*Correspondence: zhaojy@fudan.edu.cn
https://doi.org/10.1016/j.celrep.2021.109821

SUMMARY

Elevation in homocysteine (Hcy) level is associated with insulin resistance; however, the causality between them and the underlying mechanism remain elusive. Here, we show that Hcy induces insulin resistance and causes diabetic phenotypes by protein cysteine-homocysteinylation (C-Hcy) of the pro-insulin receptor (pro-IR). Mechanistically, Hcy reacts and modifies cysteine-825 of pro-IR in the endoplasmic reticulum (ER) and abrogates the formation of the original disulfide bond. C-Hcy impairs the interaction between pro-IR and the Furin protease in the Golgi apparatus, thereby hindering the cleavage of pro-IR. In mice, an increase in Hcy level decreases the mature IR level in various tissues, thereby inducing insulin resistance and the type 2 diabetes phenotype. Furthermore, inhibition of C-Hcy *in vivo* and *in vitro* by overexpressing protein disulfide isomerase rescues the Hcy-induced phenotypes. In conclusion, C-Hcy in the ER can serve as a potential pharmacological target for developing drugs to prevent insulin resistance and increase insulin sensitivity.

INTRODUCTION

Insulin resistance is a fundamental pathogenic state associated with various metabolic disorders, including obesity and type 2 diabetes. Several studies have shown that resistance to the pleiotropic effects of insulin represents a key process in the development of the disease (Brüning et al., 1997; Froguel et al., 1993; Kahn, 1994; Martin et al., 1992); however, the underlying molecular mechanisms of insulin resistance are only partially understood and are heterogeneous in nature. Furthermore, although genetic mutations, including those in *INSR*, *HNF1A*, *TRPM6*, *CAPN10*, *HMGA1*, *LIN28a/b*, and *GLUT4*, are the known causes of rare and severe insulin resistance (Hosoe et al., 2017; Low et al., 2021; Nair et al., 2012; Chiefari et al., 2011; Sáez et al., 2008; Wandel et al., 1995; Zhu et al., 2011), dysregulation of cell metabolism can also lead to insulin resistance in various ways. For example, several clinical studies have shown that elevated levels of circulating amino acids, including homocysteine (Hcy) and branched-chain amino acids (Jang et al., 2016; Wang et al., 2011), and high levels of circulating lipids and free fatty acids (Adiels et al., 2008; Chu et al., 2013; Wilding, 2007) play important roles in the development of insulin resistance and are associated with an increased risk of diabetes.

Hcy is a naturally occurring sulfur-containing amino acid, and elevation in its level is observed in various diseases (Brustolin

et al., 2010). Patients with type 2 diabetes have significantly higher plasma Hcy levels (Ala et al., 2017; Joshi et al., 2016; Meigs et al., 2001). Various studies have also revealed a positive correlation between Hcy levels and the degree of insulin resistance in patients with hypothyroidism or polycystic ovary syndrome (Yang et al., 2015; Yilmaz et al., 2008). However, whether elevated Hcy level in humans is the cause or consequence of insulin resistance and type 2 diabetes remains controversial (Yang et al., 2015; Zhang et al., 2018). Several studies have shown that Hcy elevation is the cause of type 2 diabetes; for example, results from *in vivo* and *in vitro* experiments have shown that elevation in the Hcy level causes insulin resistance (Li et al., 2008, 2013) and that Hcy-lowering therapy is beneficial for patients with type 2 diabetes (Elbarbary et al., 2020). However, the causality between Hcy and insulin resistance is still controversial, as the underlying mechanism remains elusive so far.

Hcy is a key metabolite of the one-carbon metabolism pathway. Hcy is generated from the hydrolysis of S-adenosylhomocysteine, a methylation product, and cannot be completely used by cells. Hcy removal is catalyzed by remethylation, *trans*-sulfuration, and Hcy-thiolactone (HTL) pathways. Hcy remethylation to methionine is catalyzed by the methionine synthase (MTR) (Li et al., 1996), which links the folate cycle with Hcy metabolism, and the betaine-Hcy methyltransferase (BHMT) (Sunden et al., 1997), which is mainly expressed in the liver and kidneys. Hcy *trans*-sulfuration is facilitated by the action

of the following two vitamin B6-dependent enzymes: cystathionine β-synthase (CBS) and cystathionine γ-lyase (CTH) (Nazki et al., 2014; Moreover, Hcy could be converted to HTL in a reaction catalyzed by methionyl-tRNA synthetase (MARS) (Jakubowski, 2019). Interestingly, high levels of Hcy correlated with an increased risk of insulin resistance and diabetes have been reported in clinical observations. In contrast, methionine and cysteine have not been reported to be associated with these phenotypes; although, they are downstream metabolites of Hcy and are the structural analogs of Hcy (sulfur-containing amino acid). These facts suggest that Hcy induces insulin resistance by its role in signaling, instead of in metabolism.

We have previously showed that Hcy can modify proteins and alter their functions, indicating that Hcy is involved in cell signaling. We observed that Hcy modified the lysine residue of proteins and signaled by the formation of protein lysine-Hcy (K-Hcy). K-Hcy inhibited superoxide dismutase 1 (SOD1) and SOD2 activities and increased the levels of reactive oxygen species (Mei et al., 2020). In addition, K-Hcy inactivates the ATR-mediated DNA damage repair pathway, resulting in the accumulation of DNA damage (Wang et al., 2018). Based on these observations, we hypothesized that Hcy might regulate insulin signaling through its signal molecular role. In this study, we investigated the mechanism of how Hcy caused insulin resistance *in vitro* and *in vivo*. We observed that instead of lysine-homocysteinylation, Hcy reacted with the pro-insulin receptor (pro-IR) at critical cysteine residues to form protein cysteine-Hcy (C-Hcy). The C-Hcy modification of pro-IR prevented its interaction with the Furin protease, limiting its cleavage and maturation and causing insulin resistance.

RESULTS

Hcy causes insulin resistance by decreasing IR abundance

We first investigated the role of Hcy in insulin signaling in insulin-sensitive cell lines, including the normal human liver cell line (LO2) (Geng et al., 2018), human liver cancer cell line (HepG2) (Gong et al., 2016), mouse skeletal muscle cell line (C2C12) (Sim et al., 2019), rat cardiac muscle cell line (H9c2) (Zhang et al., 2014), mouse cardiac muscle cell line (HL-1) (Hartmann et al., 2016), and Chinese hamster ovary cell line (CHO) (Hosoe et al., 2017), through monitoring glucose uptake and protein levels of the insulin signaling pathway. We observed that although treatment of cells with insulin increased the glucose uptake of cells, an increase in Hcy levels in culture media blocked the effect of insulin and led to reduced glucose uptake in C2C12 and HL-1 cells (Figure 1A). An assessment of the protein and phosphorylation levels of insulin signaling pathway proteins revealed that an increase in the Hcy level inhibited this pathway in both a time- and dose-dependent manner. This result was indicated by the reduction in the phosphorylation levels of insulin receptor beta subunit (IR-β), AKT2, and AS160 and decrease in the protein levels of IR alpha (IR-α) and beta (IR-β) subunits in HepG2 (Figures 1B and 1C) and HL-1 cells (Figures S1A, S1B, and S1C). Considering that the relative phosphorylation levels of IR-β did not change after Hcy treatment (Figures 1B and 1C; Figures S1A and S1B) and that overexpression of IR rescued

the insulin pathway (Figure 1D) and glucose uptake in Hcy-treated cells (Figure S1D), we concluded that a reduction in IR-α and IR-β abundance led to insulin resistance when the Hcy level increased.

The mRNA level of IR was not affected by an elevation in Hcy level (Figure S1E), excluding the possibility that the levels of mature IR were regulated at the transcriptional level. Furthermore, treatment of HepG2 cells with the proteasome inhibitor MG132 or autophagy inhibitor chloroquine did not diminish the difference in IR-β protein levels between Hcy-treated cells or normal cells, indicating that Hcy did not alter the degradation of IR (Figures S1F and S1G). Interestingly, we observed that the abundance of the precursor of IR (pro-IR) increased in the Hcy-treated insulin-sensitive cell lines, including LO2, HepG2, C2C12, H9c2, and HL-1 cells, accompanied by a decrease in IR-β level (Figure 1E). We also found that Hcy promoted the elevation in pro-IR levels in a time- and dose-dependent manner (Figures 1B and 1C). These findings showed that Hcy inhibited the maturation of pro-IR.

Hcy impairs the maturation of pro-IR and detains pro-IR in the ER and Golgi apparatus

To investigate the mechanism by which Hcy impaired pro-IR maturation, we detected the total IR levels in organelles required for IR maturation, including in the Golgi apparatus and endoplasmic reticulum (ER). Using immunostaining in CHO cells, we observed that total IR accumulated in both the Golgi apparatus and ER in Hcy-treated cells (Figures 1F and 1G). Meanwhile, the total IR amount decreased in the cell membrane (Figure 1F). To further assess the levels of different forms of IR, we checked IR abundance in the isolated cell membrane, Golgi apparatus, and ER from LO2 cells treated with or without Hcy. The findings showed that an increase in Hcy level led to a decrease in mature IR-β level and an increase in the precursor pro-IR level in the cell membrane (Figure 1H), Golgi apparatus (Figure 1I), and ER (Figure 1J). Collectively, these results showed that Hcy inhibited cleavage, an important process in pro-IR maturation.

Hcy downregulates pro-IR cleavage by cysteine-homocysteinylation

Unlike Hcy, the addition of methionine, cystathionine, cysteine, glutathione, or HTL, the downstream metabolites of Hcy, neither decreased the levels of mature IR-β nor increased the precursor pro-IR (Figure S2A), suggesting that the pathological effect of Hcy-induced insulin resistance might not be due to its role in metabolism. Furthermore, the findings showed that although HTL did not alter the maturation of pro-IR, it exhibited a significant inhibitory effect on the phosphorylation levels of IR-β and AKT2 (Figure S2A). Consistent with our study, Najib and Sánchez-Margalet (2001, 2005) have shown that HTL negatively affects insulin signaling. Taken together, we inferred that Hcy and HTL could inhibit insulin signaling through different pathways.

We next investigated whether Hcy regulated pro-IR maturation by its role in cell signaling. Our previous studies have revealed that Hcy participates in cell signaling by lysine-homocysteinylation of target proteins (Wang et al., 2018). However, in this study, the overexpression of MARS, which generates the lysine-homocysteinylation modification, did not alter
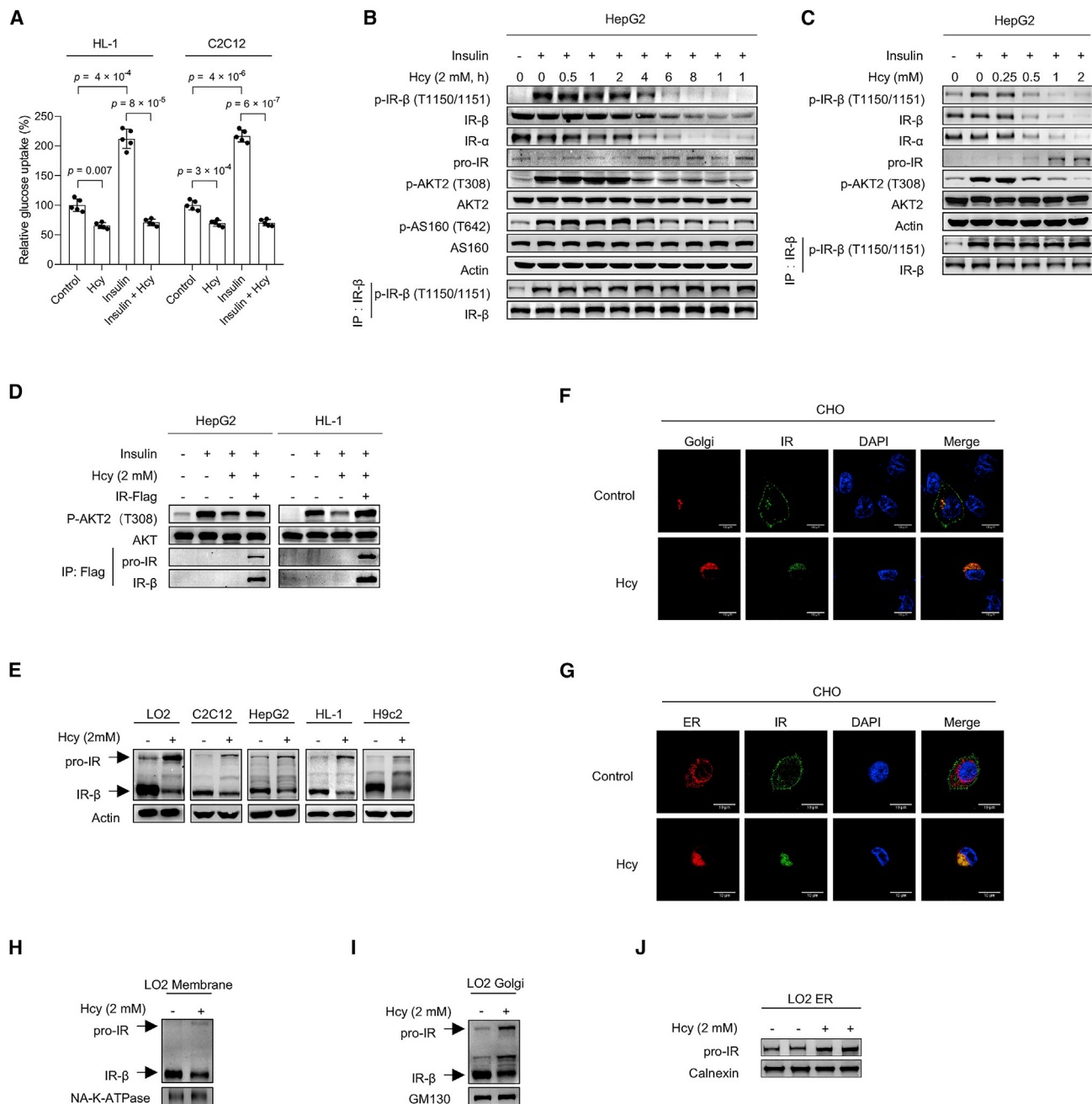
Figure 1. Homocysteine (Hcy) causes insulin resistance by impairing the cleavage of the pro-insulin receptor

(A) Glucose uptake in HL-1 and C2C12 cells with various treatments (n = 5 for each group).

(B and C) Hcy inhibits the insulin pathway in both a time-dependent (B) and dose-dependent (C) manner in HepG2 cells (n = 3 biological repeats).

(D) AKT phosphorylation levels of cells after various treatments (n = 3 biological repeats).

(E) The abundance of the pro-insulin receptor (pro-IR) and insulin receptor β (IR-β) in LO2, C2C12, HepG2, HL-1, and H9c2 cells, treated with or without Hcy (n = 3 biological repeats).

(F) Double immunofluorescence staining of the Golgi apparatus and IR in CHO cells (n = 3 biological repeats, scale bars: 10 μM).

(G) Double immunofluorescence staining of ER and IR in CHO cells (n = 3 biological repeats, scale bars: 10 μM).

(H–J) The abundance levels of pro-IR and IR-β in the separated LO2 cell membrane (H), Golgi apparatus (I), and ER (J) (n = 3 biological repeats). Data are presented as mean ± standard deviation (SD). p values were determined by one-way ANOVA with Bonferroni post hoc test.

the IR signaling pathway. Therefore, the possibility that protein lysine-homocysteinylation contributed to the Hcy-mediated regulation of pro-IR cleavage was excluded (Figure S2B). Reportedly, Hcy has been shown to modify cysteine residues in proteins by disulfide bond formation (Glushchenko and Jacobsen, 2007). Therefore, we tested whether Hcy could affect pro-IR maturation through its thiol group by using the drug affinity responsive target stability (DARTS) assay. The results showed that thiol-containing Hcy, but not sulfur-containing methionine and cystathionine (which acted as the negative controls), could bind to pro-IR (Figure 2A). Additionally, surface plasmon resonance (SPR) analysis confirmed that Hcy had a higher binding affinity to pro-IR than methionine and cystathionine (Figure S2C). These results suggested that Hcy might react with pro-IR through its thiol group and thus regulate pro-IR cleavage.

The cleavage of pro-IR consists of the following two steps: one is correct folding in ER by disulfide bond formation and the other involves cleavage in the Golgi apparatus by the proprotein convertase Furin for proteins entering the secretory pathway (Gorden et al., 1989). As Hcy modified cysteine residues in proteins by disulfide bond formation (Glushchenko and Jacobsen, 2007), and the oxidative state of ER is suitable for disulfide bond formation (Haataja et al., 2016; Sevier et al., 2007), we hypothesized that Hcy could modify the cysteine residues of pro-IR, disturb the formation of correct disulfide bonds within pro-IR, and finally impair pro-IR cleavage. To validate this hypothesis, we first screened C-Hcy sites within pro-IR by using liquid chromatography, followed by tandem mass spectrometry analysis. Multiple cysteine sites modified by Hcy were identified (Figure 2B; Figure S2D). Subsequently, using an *in vitro* assay, we validated that Hcy modified all the cysteine residues of the synthetic IR peptides containing each site (Figure 2C; Figure S2E). To identify the site or sites that contribute to the response of pro-IR to Hcy levels, we mutated each cysteine to alanine within pro-IR and tested the response of each of these mutants to Hcy levels. We observed that the pro-IR C825A mutant abrogated the ability of Hcy to hinder pro-IR maturation, as shown by the decrease in IR-β levels and accumulation of pro-IR (Figure 2D). We also confirmed that Hcy does not modify the synthetic C825A mutant IR peptide *in vitro* (Figure 2E). In addition, the fact that Hcy cannot homocysteinylate the synthetic IR peptide with the existing C825-C834 disulfide bond confirmed that Hcy competed for disulfide bond formation by C-Hcy modification before the correct disulfide bond is formed in the ER (Figure 2E). Moreover, in the pro-IR C834A mutant that disrupted the C825-C834 disulfide bond formation, we found that the cleavage efficiency of pro-IR decreased significantly and no longer responded to the increased Hcy levels (Figure 2F). These findings indicate that Hcy reacts and modifies cysteine-825 of pro-IR and impairs the cleavage of pro-IR.

Hcy concentration and PDI abundance determine the formation of the correct disulfide bond in pro-IR

The fact that thiol-containing chemical metabolites can modify the cysteine residues of proteins in the ER attracted our attention. We inquired whether free cysteine also impaired pro-IR maturation and led to insulin resistance by modifying the cysteine residues of proteins. We observed that although

cysteine could modify the cysteine residue of IR *in vitro* (Figure S3A), it did not inhibit insulin signal in a similar manner as Hcy (Figures S3B, S3C, and S3D). Besides, we confirmed that cysteine and other thiol-containing metabolites, for example, glutathione, cannot rescue the pro-IR cleavage inhibition induced by Hcy (Figure S3E). These results suggested that the disulfide bond between Hcy and pro-IR was stable. It is known that the protein disulfide isomerase (PDI) family of proteins rectifies the formation of incorrect disulfide bonds in the ER. In this study, PDI removed both C-Hcy and C-cysteine (C-Cys) modification of peptides *in vitro* (Figure 3A), and its efficiency in removing C-Cys modification was significantly higher than that of the C-Hcy modification (Figure 3A). Using an *in vitro* assay, we further confirmed that the presence of PDI decreased the efficiency of C-Hcy formation and strongly blocked the C-Cys formation, compared to the efficiencies of C-Hcy and C-Cys formation in the absence of PDI (Figure S3F). In cultured cells, the interactions between PDI and pro-IR were confirmed using co-immunoprecipitation assays, which were performed using either exogenous PDI and pro-IR proteins in HepG2 cells (Figure 3B) or endogenous PDI and pro-IR proteins in LO2 cells (Figure 3C). We also showed that the C825-Hcy modification levels of pro-IR were decreased significantly in PDI-overexpressing HepG2 cells compared to those of control cells (Figure 3D). Accordingly, overexpression of PDI in HepG2 cells reversed the effects of Hcy, including a decrease in IR-β level in the membrane (Figure 3E) and an increase in pro-IR level in the Golgi apparatus (Figure 3F) and ER (Figure 3G). Furthermore, the phenotypes of HepG2 and LO2 cells with PDI knockdown were similar to those observed after Hcy treatment, including accumulation of pro-IR, decreased mature IR levels, and inhibition of insulin signaling (Figure S3G). Collectively, these results indicated that the equilibrium of the thiol-disulfide exchange reaction catalyzed by PDI is suitable for cysteine but not for Hcy. In addition, the results also showed that an increased level of Hcy competed with disulfide bond formation on pro-IR by the formation of C-Hcy modification, and this process could be rescued by enhancing the PDI-catalyzed removal of C-Hcy.

Cysteine-homocysteinylation of pro-IR hinders the cleavage catalyzed by Furin

Pro-IR is cleaved into IR-α and -β subunits by Furin, a ubiquitously expressed transmembrane protein, which is abundant in the Golgi apparatus, where it functions to cleave other proteins into their mature/active forms. Here, we investigated whether Furin was involved in Hcy-induced pro-IR cleavage deficiency. First, although an increase in Hcy did not affect Furin abundance (Figure S3H), it reduced the interactions between Furin and pro-IR, as indicated by co-immunoprecipitation assays for which we used either an exogenous protein in HepG2 cells (Figure 3H) or endogenous proteins in LO2 cells (Figure 3I). Furthermore, using an *in vitro* assay, we confirmed that Hcy impaired the interaction between purified eukaryotic Furin and pro-IR (Figure 3J). These results indicated that Hcy abrogated pro-IR cleavage by impairing the interaction between Furin and pro-IR. Second, in Hcy-treated cells, overexpression of Furin did not increase the production of the mature version of IR-α and -β, which had been downregulated by Hcy, suggesting that the formation of
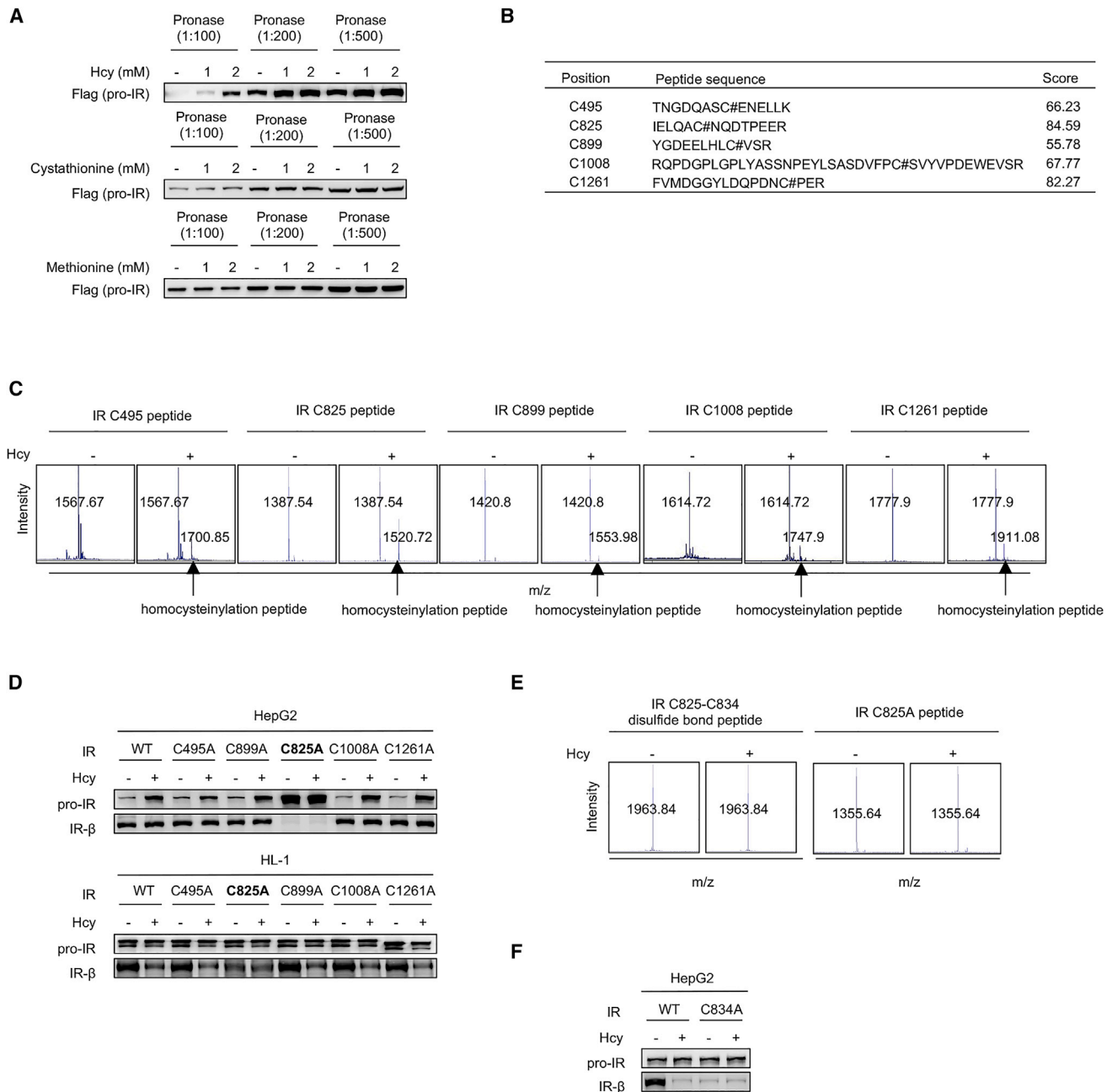
Figure 2. Hcy downregulates pro-IR cleavage by cysteine-homocysteinylation

(A) Drug affinity responsive target stability (DARTS) assay showing the binding potential of Hcy, cystathionine, and methionine to pro-IR.

(B) Multiple cysteine sites within pro-IR are identified to be homocysteinylated. The mass spectrum is shown in Figure S2D.

(C) The *in vitro* assay shows that Hcy modifies cysteine residues of IR identified in the mass spectrum. The purity and sequence of peptides used are provided in Figure S2E.

(D) The cleavage efficiencies of different IR mutants in HepG2 and HL-1 cells (n = 3 biological repeats).

(E) The *in vitro* assay shows that Hcy cannot modify the C825 residue when the C825-C834 disulfide bond is formed in the IR peptide (left panel) and the peptide that mutates C825 to alanine (right panel). The information (purity and sequences) regarding peptides used is provided in Figure S2E.

(F) The cleavage efficiency of IR C834A mutant in HepG2 cells (n = 3 biological repeats).

the correct disulfide bond was crucial for the cleavage (Figure S3I). In contrast, Furin knockdown resulted in the accumulation of pro-IR, although the levels of Hcy in the culture medium did not increase (Figure 3K). Moreover, PDI rescued the Hcy-mediated inhibition of the insulin pathway; however, it failed to rescue the insulin pathway in Furin knockdown cells (Figure 3L).
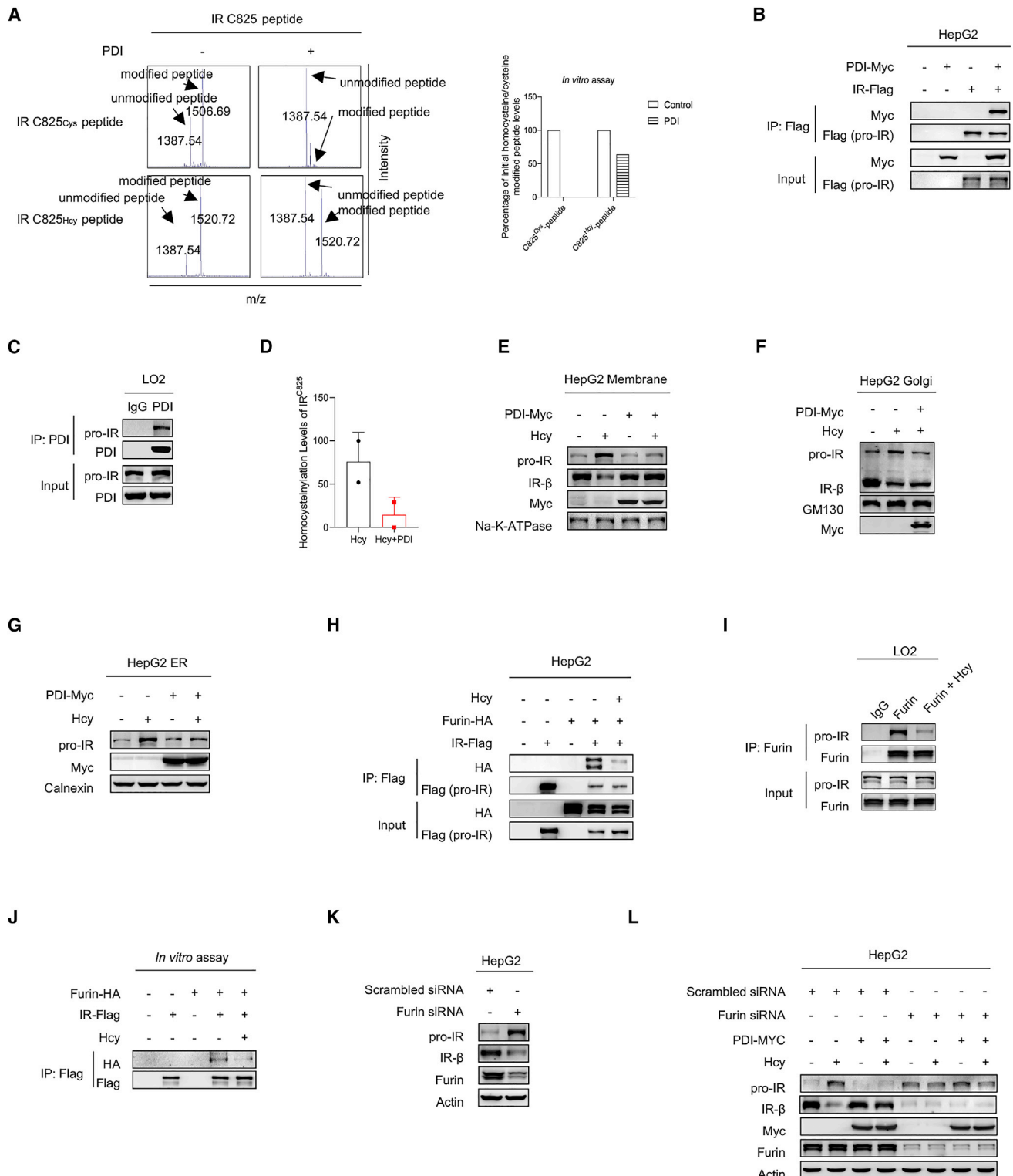
Figure 3. Hcy concentration and PDI abundance determine the formation of the correct disulfide bond in pro-IR

(A) The *in vitro* assay shows PDI is more efficient in removing C-Cys modification than in removing C-Hcy modification.

(B) Co-immunoprecipitation assay showing the interaction of exogenous PDI and exogenous pro-IR in cultured HepG2 cells.

(C) Co-immunoprecipitation assay showing the interaction of endogenous PDI and endogenous pro-IR in cultured LO2 cells.

(D) C825-Hcy modification levels of pro-IR in PDI-overexpression HepG2 and normal HepG2 cells. Data are presented as mean ± SD (n = 2 biological repeats).

(legend continued on next page)

These findings suggested the important role of Furin in cleavage of pro-IR into its mature/active forms.

Increased Hcy causes insulin resistance by impairing pro-IR cleavage in mice

As elevation in Hcy level frequently occurs in humans and is associated with various pathologies, we next examined whether an increase in Hcy level induced insulin resistance by blocking pro-IR cleavage in mice. We fed 6-week-old male mice with either high-Hcy chow or normal chow. The plasma Hcy concentration in the Hcy-fed group (19.56 ± 0.95 μmol/L) increased by 30%, compared to that in the normal chow-fed group (14.96 ± 1.04 μmol/L) (Figure 4A). After mice fed for 4 months (Figures S4A–S4F), the fasting blood glucose levels of male mice in the Hcy-fed group were significantly higher than those of the male mice in the control group (Figure 4B). Glucose tolerance tests (GTTs) and insulin tolerance tests (ITTs) revealed that high levels of Hcy impaired glucose tolerance (Figure 4C) and insulin sensitivity in mice (Figure 4D). Furthermore, concordant with the clinical symptoms that the patients with insulin resistance exhibit increased fasting blood insulin, we observed that increased levels of fasting pro-insulin, fasting insulin, and fasting C-peptide in Hcy-fed mice caused insulin resistance by using the enzyme-linked immunosorbent assay (ELISA) and western blotting (Figures S4G and S4H). Next, we analyzed the insulin signaling status in mouse tissue. We observed that the IR-β level decreased in the tissues of mice (including muscle, adipose, and liver) of the Hcy-fed group compared to that in the normal-chow-fed group (Figure 4E). Although the pro-IR levels did not increase significantly in tissues from Hcy-high mice (Figure 4E), the ratio of IR-β to pro-IR decreased considerably (Figure 4F), indicating that pro-IR maturation was impaired in tissues of Hcy-fed mice. We also verified that compared to that in normal-chow-fed mice, IR phosphorylation did not respond to insulin stimulation in insulin-sensitive tissues of Hcy-fed mice because of a considerable decrease in the amount of mature IR-β (Figure 4G).

Inhibition of cysteine-homocysteinylation refreshes the insulin signal

As PDI was able to remove C-Hcy modification on pro-IR and activate the IR signal (see Figure 3), we next investigated whether inhibition of C-Hcy formation could refresh the insulin signal in the mouse model. First, we overexpressed PDI in muscle, adipose, and liver tissues of mice through local or tail injection of adeno-associated virus (AAV)-PDI. The GTTs and ITTs revealed that in the Hcy-fed mouse model, overexpression of PDI in these tissues (muscle: Figures 5A, 5B, and 5C; adipose: Figures 5D, 5E, and 5F; and liver: Figures 5G, 5H, and 5I) was able to partially rescue the insulin tolerance and sensitivity that were impaired by

high levels of Hcy. As shown in Figure 4, increased Hcy impaired insulin signaling in various tissues, including muscle, liver, and adipose tissues. Taken together, it can be inferred that IR levels in these tissues play non-negligible roles in insulin resistance. Accordingly, in the Hcy-fed mouse model, we found that global overexpression of PDI in mice through intravenous injection of AAV-PDI by the tail was able to rescue all the phenotypes induced by Hcy, including glucose tolerance (Figure 5J) and insulin tolerance (Figure 5K), increase in fasting blood glucose level (Figure S5A), and decrease in IR-β level in insulin-sensitive tissues (Figure 5L). We also validated those findings in the Hcy-fed mouse model; increased IR abundance through intravenous injection of AAV-INSR by the tail could rescue all the phenotypes induced by Hcy (Figures S5B and S5C). Taken together, our findings revealed that Hcy could inhibit the pro-IR maturation by the formation of C-Hcy and inhibition of cysteine-homocysteinylation could refresh the insulin signal (Figure 5M).

DISCUSSION

Elevation in Hcy levels is associated with important cellular phenotypes and many diseases, although its pathological role is not clearly understood. Although many studies have reported that an increase in Hcy levels predicts the onset of diabetes or is observed in patients with diabetes, some studies have suggested that Hcy elevation was the result of insulin resistance. Therefore, the causality between Hcy and insulin resistance is a controversial point. Furthermore, the elevation of Hcy level correlates with certain important cellular phenotypes, including the increase in reactive oxygen species level (Mei et al., 2020) and DNA damage (Wang et al., 2018), and several diseases, including birth defects (Wang et al., 2017; Zhao et al., 2012, 2013, 2014), various kinds of cancers (Liu et al., 2018; Tastekin et al., 2015; Wang et al., 2018), cardiovascular diseases (McCully, 2015), and neurodegenerative diseases (Moretti and Caruso, 2019). Taken together, although Hcy is known as a "universal" causative metabolite, which has been associated with the onset of various diseases for a long time, progress in determining the pathological role of Hcy was limited because of a lack of knowledge regarding the mechanism by which Hcy induced these diseases. In this study, we observed that Hcy reacted with pro-IR at critical cysteine residues to form C-Hcy. Using *in vitro* assays, cultured cells, and a mouse model, we found that the C-Hcy modification of pro-IR prevents its interaction with the Furin protease, limiting its cleavage and maturation and causing insulin resistance. Altogether, this study provides a mechanistic explanation for the link between an elevated Hcy level and insulin resistance.

In cells, Hcy modifies the cysteine residues of proteins spontaneously in a non-enzymatic manner. The C-Hcy modification

---

(E–G) The abundance of pro-IR and IR-β in the cell membrane (E), Golgi apparatus (F), and endoplasmic reticulum (ER) (G) from PDI-overexpressing HepG2 cells and control cells treated with or without Hcy.

(H) Co-immunoprecipitation assay showing the interaction of exogenous Furin and pro-IR in cultured HepG2 cells treated with or without Hcy.

(I) Co-immunoprecipitation assay showing the interaction of endogenous Furin and pro-IR in cultured LO2 cells treated with or without Hcy.

(J) The interaction between eukaryotic purified Furin and pro-IR *in vitro*.

(K) The abundance of pro-IR and IR-β in HepG2 cells with Furin knockdown and control cells.

(L) The abundance of pro-IR and IR-β in HepG2 and control cells with Furin knockdown, transfected with or without PDI. Three biological replicates were used for Figures 3B, 3C, 3E, 3F, 3G, 3H, 3I, 3J, 3K, and 3L.
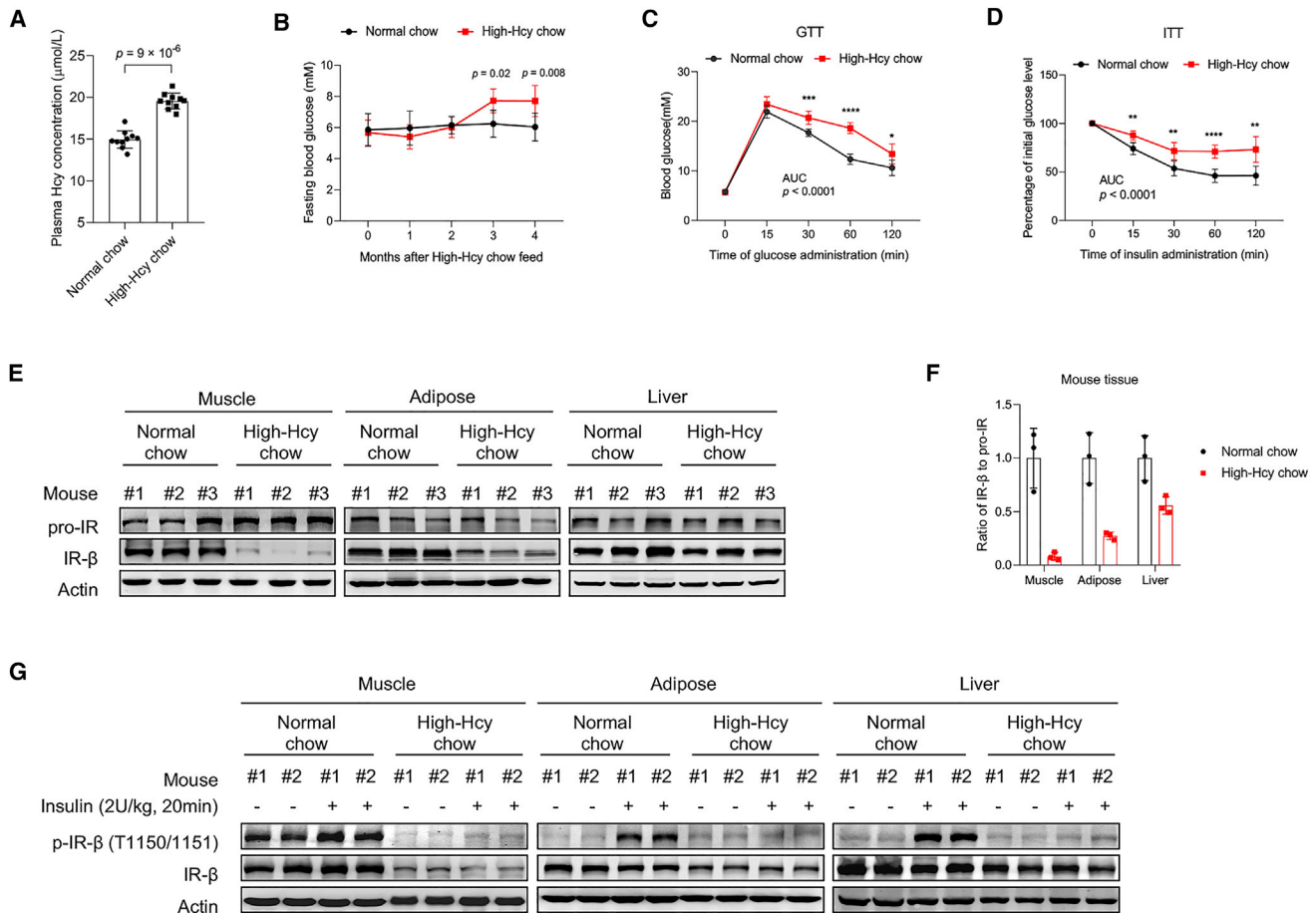
Figure 4. Increased Hcy causes insulin resistance by impairing pro-IR cleavage in mice

(A–D) Hcy (n = 10 for each group) (A), fasting blood glucose (B), glucose tolerance test (GTT) (C), and insulin tolerance test (ITT) (D) levels in mice fed with high-Hcy chow or normal chow (n = 6 for each group in B, C, and D).

(E) The levels of pro-IR and IR-β in various tissues of mice fed either high-Hcy chow or normal chow.

(F) The ratio of IR-β to pro-IR indicating the cleavage efficiency of pro-IR in various tissues of mice fed either high-Hcy chow or normal chow (n = 3 for each group).
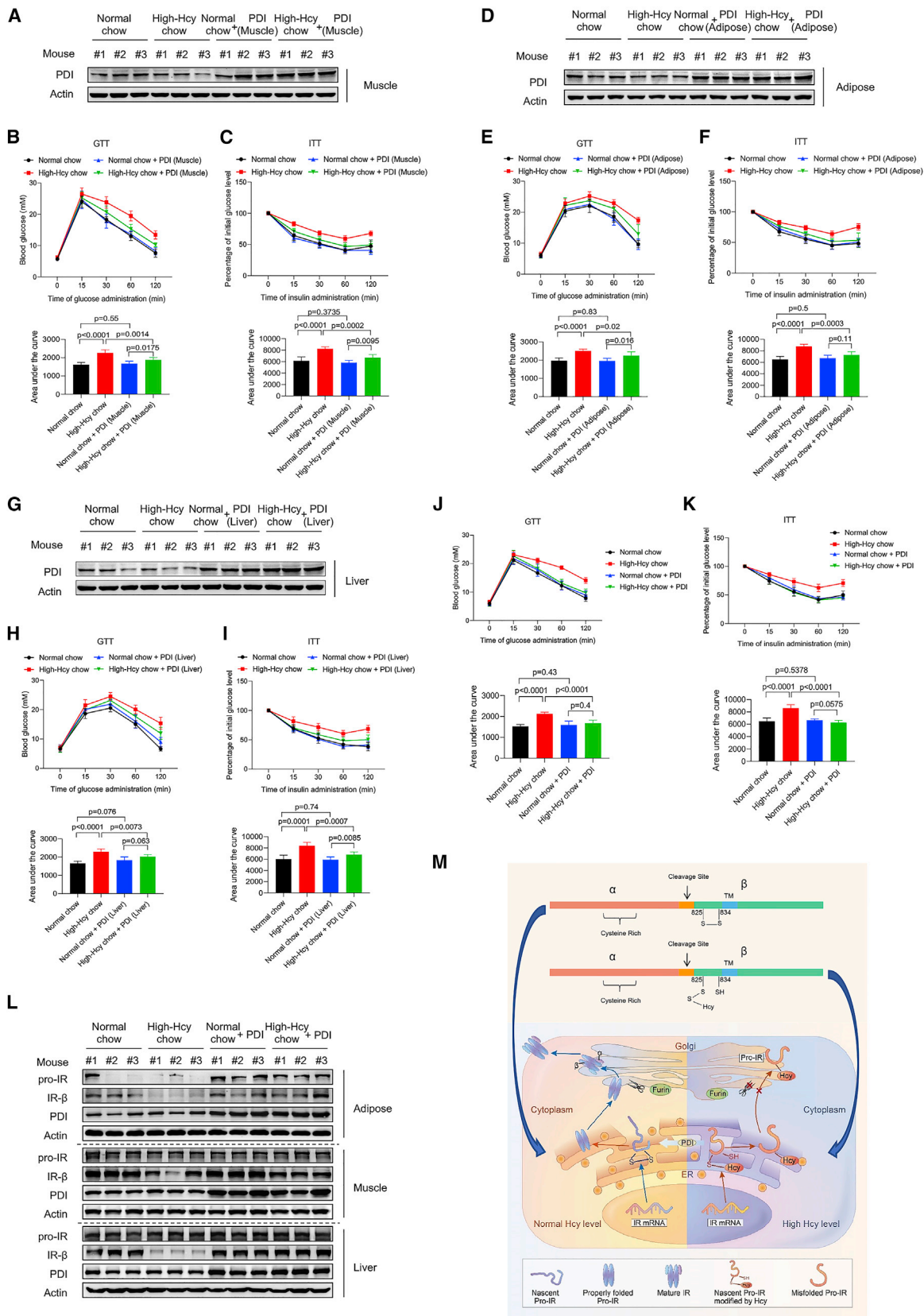
(G) The phosphorylation and expression levels of IR in various tissues of mice fed either high-Hcy chow or normal chow. Data are presented as mean ± SD. *p < 0.05, **p < 0.01, ***p < 0.001 versus the control group according to Student's t test. For GTT and ITT, two-way ANOVA with multiple comparisons were performed for statistical analyses.

occurs mainly in the ER because of the latter's oxidative state. As a result, Hcy affects many proteins that participate in disulfide-bond-mediated processes in the ER by C-Hcy modification. We also confirmed that Hcy affected Notch1 and IGF1R, which are other kinds of membrane proteins involved in disulfide-bond-mediated processes in the ER. An increase in the Hcy level in HL-1 cells reduced mature Notch1 levels, whereas it increased Notch1 precursor levels (Figure S5D). Furthermore, an increased Hcy level in HEK293T cells also increased pro-IGF1R and decreased mature IGF1R levels (Figure S5E).

Interestingly, responders can sense intracellular Hcy by different protein post-translational modifications. With the exception of the dynamically changing levels of Hcy, the protein lysine-homocysteinylation levels can be determined from the modification catalyzed by MARS. In contrast, protein C-Hcy levels were determined from the de-modification process catalyzed by PDI but not from the modification process. These observations suggested that different upstream signals participate in generating the Hcy signal. Lysine-homocysteinylation was regulated by MARS, which responded to genetic (for example, gene copy number; Mei et al., 2020) and nutritional signals (for example, high-fat diet; Wang et al., 2018). However, the upstream signal of PDI is still unknown. A previous study had revealed the cross-talk of lysine and cysteine homocysteinylation in blood proteins (Glowacki and Jakubowski, 2004). Therefore, identifying the intracellular upstream regulator of PDI under physiological conditions and determining whether lysine and cysteine homocysteinylation cross talk require further studies.

The IR is a tetrameric protein consisting of two extracellular α subunits and two transmembrane β subunits joined by disulfide bonds. Both subunits are generated from a single large precursor by proteolytic cleavage. The IR recognizes and binds insulin, thereby transmitting the insulin signal inside the cells. Precise modulation of IR is vital for adaptation as individuals move

from the fed to the fasted state. The positive and negative modulators acting on different steps of IR expression ensure a proper and coordinated biological response to insulin in different tissues. Here, we identified a metabolic regulation of IR in addition to mutations (Takahashi et al., 2010) and transcription, translation, and protein degradation (Lay et al., 2017). Our finding demonstrating considerable inhibition of the cleavage and maturation of pro-IR by a high level of Hcy suggested that imbalance in one-carbon metabolism contributed to insulin resistance and type 2 diabetes, as a high level of Hcy can be caused by either increased intracellular methylation levels or reduced intracellular folate levels. More importantly, we observed that blocking C-Hcy formation by enhancing PDI activity increased the IR protein level and prevented the development of insulin resistance in cultured cells, as well as relieved insulin resistance and reduced blood glucose level in a Hcy-fed mouse model. In conclusion, it is evident from these *in vitro* and *in vivo* results that C-Hcy modification in the ER could be an ideal pharmacological target for the development of drugs to prevent insulin resistance and increase insulin sensitivity.

STAR★METHODS

Detailed methods are provided in the online version of this paper and include the following:

- ● KEY RESOURCES TABLE
- ● RESOURCE AVAILABILITY
  - ○ Lead contact
  - ○ Materials availability
  - ○ Data and code availability
- ● EXPERIMENTAL MODEL AND SUBJECT DETAILS
  - ○ Tissue cell lines
  - ○ Mouse model
- ● METHOD DETAILS
  - ○ Plasmid construction
  - ○ Cell transfections and co-immunoprecipitation
  - ○ Reverse transcription and quantitative reverse transcription-PCR (qRT-PCR)
  - ○ Western blotting
  - ○ Immunofluorescence
  - ○ Glucose uptake
  - ○ Drug affinity responsive target stability
  - ○ Surface plasmon resonance
  - ○ PDI purification
  - ○ *In vitro* modification
  - ○ *In vitro* de-modification
  - ○ Sample preparation and liquid chromatography-tandem mass spectrometry (LC-MS)/MS analysis
  - ○ C-Hcy site identification
  - ○ Cellular fractionation
  - ○ Insulin and glucose tolerance tests
  - ○ Plasma insulin, proinsulin, and C-peptide detection
  - ○ Hcy quantification
- ● QUANTIFICATION AND STATISTICAL ANALYSIS

AUTHOR CONTRIBUTIONS

J.-Y.Z. conceived the concept and designed and supervised the experiments; X.Z., Y.-Y.Q., L.L., Y.-N.Q., H.-R.G., Y.L., W.X., and J.C. performed the experiments; J.-Y.Z. wrote the manuscript. All authors read and discussed the manuscript.

DECLARATION OF INTERESTS

The authors declare no competing interests.

REFERENCES

Adiels, M., Olofsson, S.O., Taskinen, M.R., and Borén, J. (2008). Overproduction of very low-density lipoproteins is the hallmark of the dyslipidemia in the metabolic syndrome. Arterioscler. Thromb. Vasc. Biol. *28*, 1225–1236.

Ala, O.A., Akintunde, A.A., Ikem, R.T., Kolawole, B.A., Ala, O.O., and Adedeji, T.A. (2017). Association between insulin resistance and total plasma

Figure 5. Inhibition of cysteine-homocysteinylation refreshes the insulin signal
(A–C) The abundance of PDI in muscle (A), GTT (B), and ITT (C) analysis of high-Hcy chow or normal-chow-fed mice receiving a local injection of AAV2-CMV_bGI-PDIA1-MCS or control virus (n = 6 for each group).
(D–F) The abundance of PDI in adipose (D), GTT (E), and ITT (F) analysis of high-Hcy-chow-fed or normal-chow-fed mice with local injection with AAV2-hAdp-PDIA1-MCS-EGFP-WPRE-SV40pA or control virus (n = 6 for each group).
(G–I) The abundance of PDI in the liver (G), GTT (H), and ITT (I) analysis of high-Hcy-chow-fed or normal-chow-fed mice receiving an intravenous injection of AAV2-hTBG-PDIA1-MCS or control virus by the tail (n = 6 for each group).
(J and K) GTT (J) and ITT (K) analysis of high-Hcy-chow-fed or normal-chow-fed mice with an intravenous injection of AAV-PDI or control virus by the tail (n = 8 for each group).
(L) Abundance of pro-IR, IR-β, and PDI in adipose, muscle, and liver tissues of mice subjected to various treatments.
(M) Schematic model showing the mechanism of inhibition of pro-IR cleavage by Hcy by the formation of C-Hcy. Data are presented as mean ± SD. *p < 0.05, **p < 0.01, ***p < 0.001 versus the control group. For GTT and ITT, two-way ANOVA with multiple comparisons were performed for statistical analyses. Additionally, the area under curve (AUC) of each mouse was calculated and further evaluated by a two-tailed unpaired t test with/without Welch's correction or one-way ANOVA.

homocysteine levels in type 2 diabetes mellitus patients in south west Nigeria. Diabetes Metab. Syndr. *11*, S803–S809.

Brüning, J.C., Winnay, J., Bonner-Weir, S., Taylor, S.I., Accili, D., and Kahn, C.R. (1997). Development of a novel polygenic model of NIDDM in mice heterozygous for IR and IRS-1 null alleles. Cell *88*, 561–572.

Brustolin, S., Giugliani, R., and Félix, T.M. (2010). Genetics of homocysteine metabolism and associated disorders. Braz. J. Med. Biol. Res. *43*, 1–7.

Chiefari, E., Tanyolaç, S., Paonessa, F., Pullinger, C.R., Capula, C., Iiritano, S., Mazza, T., Forlin, M., Fusco, A., Durlach, V., et al. (2011). Functional variants of the HMGA1 gene and type 2 diabetes mellitus. JAMA *305*, 903–912.

Chu, X., Liu, L., Na, L., Lu, H., Li, S., Li, Y., and Sun, C. (2013). Sterol regulatory element-binding protein-1c mediates increase of postprandial stearic acid, a potential target for improving insulin resistance, in hyperlipidemia. Diabetes *62*, 561–571.

Elbarbary, N.S., Ismail, E.A.R., Zaki, M.A., Darwish, Y.W., Ibrahim, M.Z., and El-Hamamsy, M. (2020). Vitamin B complex supplementation as a homocysteine-lowering therapy for early stage diabetic nephropathy in pediatric patients with type 1 diabetes: A randomized controlled trial. Clin. Nutr. *39*, 49–56.

Froguel, P., Velho, G., Passa, P., and Cohen, D. (1993). Genetic determinants of type 2 diabetes mellitus: lessons learned from family studies. Diabete Metab. *19*, 1–10.

Geng, S., Wang, S., Zhu, W., Xie, C., Li, X., Wu, J., Zhu, J., Jiang, Y., Yang, X., Li, Y., et al. (2018). Curcumin suppresses JNK pathway to attenuate BPA-induced insulin resistance in LO2 cells. Biomed. Pharmacother. *97*, 1538–1543.

Glowacki, R., and Jakubowski, H. (2004). Cross-talk between Cys34 and lysine residues in human serum albumin revealed by N-homocysteinylation. J. Biol. Chem. *279*, 10864–10871.

Glushchenko, A.V., and Jacobsen, D.W. (2007). Molecular targeting of proteins by L-homocysteine: mechanistic implications for vascular disease. Antioxid. Redox Signal. *9*, 1883–1898.

Gong, Q., Hu, Z., Zhang, F., Cui, A., Chen, X., Jiang, H., Gao, J., Chen, X., Han, Y., Liang, Q., et al. (2016). Fibroblast growth factor 21 improves hepatic insulin sensitivity by inhibiting mammalian target of rapamycin complex 1 in mice. Hepatology *64*, 425–438.

Gorden, P., Arakaki, R., Collier, E., and Carpentier, J.L. (1989). Biosynthesis and regulation of the insulin receptor. Yale J. Biol. Med. *62*, 521–531.

Haataja, L., Manickam, N., Soliman, A., Tsai, B., Liu, M., and Arvan, P. (2016). Disulfide Mispairing During Proinsulin Folding in the Endoplasmic Reticulum. Diabetes *65*, 1050–1060.

Hartmann, T., Overhagen, S., Ouwens, D.M., Raschke, S., Wohlfart, P., Tennagels, N., Wronkowitz, N., and Eckel, J. (2016). Effect of the long-acting insulin analogues glargine and degludec on cardiomyocyte cell signalling and function. Cardiovasc. Diabetol. *15*, 96.

Hosoe, J., Kadowaki, H., Miya, F., Aizu, K., Kawamura, T., Miyata, I., Satomura, K., Ito, T., Hara, K., Tanaka, M., et al. (2017). Structural Basis and Genotype-Phenotype Correlations of INSR Mutations Causing Severe Insulin Resistance. Diabetes *66*, 2713–2723.

Jakubowski, H. (2019). Homocysteine Modification in Protein Structure/ Function and Human Disease. Physiol. Rev. *99*, 555–604.

Jang, C., Oh, S.F., Wada, S., Rowe, G.C., Liu, L., Chan, M.C., Rhee, J., Hoshino, A., Kim, B., Ibrahim, A., et al. (2016). A branched-chain amino acid metabolite drives vascular fatty acid transport and causes insulin resistance. Nat. Med. *22*, 421–426.

Joshi, M.B., Baipadithaya, G., Balakrishnan, A., Hegde, M., Vohra, M., Ahamed, R., Nagri, S.K., Ramachandra, L., and Satyamoorthy, K. (2016). Elevated homocysteine levels in type 2 diabetes induce constitutive neutrophil extracellular traps. Sci. Rep. *6*, 36362.

Kahn, C.R. (1994). Banting Lecture. Insulin action, diabetogenes, and the cause of type II diabetes. Diabetes *43*, 1066–1084.

Lay, A.C., Hurcombe, J.A., Betin, V.M.S., Barrington, F., Rollason, R., Ni, L., Gillam, L., Pearson, G.M.E., Østergaard, M.V., Hamidi, H., et al. (2017). Prolonged exposure of mouse and human podocytes to insulin induces insulin

resistance through lysosomal and proteasomal degradation of the insulin receptor. Diabetologia *60*, 2299–2311.

Li, Y.N., Gulati, S., Baker, P.J., Brody, L.C., Banerjee, R., and Kruger, W.D. (1996). Cloning, mapping and RNA analysis of the human methionine synthase gene. Hum. Mol. Genet. *5*, 1851–1858.

Li, Y., Jiang, C., Xu, G., Wang, N., Zhu, Y., Tang, C., and Wang, X. (2008). Homocysteine upregulates resistin production from adipocytes in vivo and in vitro. Diabetes *57*, 817–827.

Li, Y., Zhang, H., Jiang, C., Xu, M., Pang, Y., Feng, J., Xiang, X., Kong, W., Xu, G., Li, Y., and Wang, X. (2013). Hyperhomocysteinemia promotes insulin resistance by inducing endoplasmic reticulum stress in adipose tissue. J. Biol. Chem. *288*, 9583–9592.

Liu, Z., Cui, C., Wang, X., Fernandez-Escobar, A., Wu, Q., Xu, K., Mao, J., Jin, M., and Wang, K. (2018). Plasma Levels of Homocysteine and the Occurrence and Progression of Rectal Cancer. Med. Sci. Monit. *24*, 1776–1783.

Low, B.S.J., Lim, C.S., Ding, S.S.L., Tan, Y.S., Ng, N.H.J., Krishnan, V.G., Ang, S.F., Neo, C.W.Y., Verma, C.S., Hoon, S., et al. (2021). Decreased GLUT2 and glucose uptake contribute to insulin secretion defects in MODY3/HNF1A hiPSC-derived mutant β cells. Nat. Commun. *12*, 3133.

Martin, B.C., Warram, J.H., Krolewski, A.S., Bergman, R.N., Soeldner, J.S., and Kahn, C.R. (1992). Role of glucose and insulin resistance in development of type 2 diabetes mellitus: results of a 25-year follow-up study. Lancet *340*, 925–929.

McCully, K.S. (2015). Homocysteine and the pathogenesis of atherosclerosis. Expert Rev. Clin. Pharmacol. *8*, 211–219.

Mei, X., Qi, D., Zhang, T., Zhao, Y., Jin, L., Hou, J., Wang, J., Lin, Y., Xue, Y., Zhu, P., et al. (2020). Inhibiting MARSs reduces hyperhomocysteinemia-associated neural tube and congenital heart defects. EMBO Mol. Med. *12*, e9469.

Meigs, J.B., Jacques, P.F., Selhub, J., Singer, D.E., Nathan, D.M., Rifai, N., D'Agostino, R.B., Sr., and Wilson, P.W.; Framingham Offspring Study (2001). Fasting plasma homocysteine levels in the insulin resistance syndrome: the Framingham offspring study. Diabetes Care *24*, 1403–1410.

Moretti, R., and Caruso, P. (2019). The Controversial Role of Homocysteine in Neurology: From Labs to Clinical Practice. Int. J. Mol. Sci. *20*, 231.

Nair, A.V., Hocher, B., Verkaart, S., van Zeeland, F., Pfab, T., Slowinski, T., Chen, Y.P., Schlingmann, K.P., Schaller, A., Gallati, S., et al. (2012). Loss of insulin-induced activation of TRPM6 magnesium channels results in impaired glucose tolerance during pregnancy. Proc. Natl. Acad. Sci. USA *109*, 11324–11329.

Najib, S., and Sánchez-Margalet, V. (2001). Homocysteine thiolactone inhibits insulin signaling, and glutathione has a protective effect. J. Mol. Endocrinol. *27*, 85–91.

Najib, S., and Sánchez-Margalet, V. (2005). Homocysteine thiolactone inhibits insulin-stimulated DNA and protein synthesis: possible role of mitogen-activated protein kinase (MAPK), glycogen synthase kinase-3 (GSK-3) and p70 S6K phosphorylation. J. Mol. Endocrinol. *34*, 119–126.

Nazki, F.H., Sameer, A.S., and Ganaie, B.A. (2014). Folate: metabolism, genes, polymorphisms and the associated diseases. Gene *533*, 11–20.

Sáez, M.E., González-Sánchez, J.L., Ramírez-Lorca, R., Martínez-Larrad, M.T., Zabena, C., González, A., Morón, F.J., Ruiz, A., and Serrano-Ríos, M. (2008). The CAPN10 gene is associated with insulin resistance phenotypes in the Spanish population. PLoS One *3*, e2953.

Sevier, C.S., Qu, H., Heldman, N., Gross, E., Fass, D., and Kaiser, C.A. (2007). Modulation of cellular disulfide-bond formation and the ER redox environment by feedback regulation of Ero1. Cell *129*, 333–344.

Sim, W.C., Kim, D.G., Lee, W., Sim, H., Choi, Y.J., and Lee, B.H. (2019). Activation of SIRT1 by L-serine increases fatty acid oxidation and reverses insulin resistance in C2C12 myotubes. Cell Biol. Toxicol. *35*, 457–470.

Sunden, S.L., Renduchintala, M.S., Park, E.I., Miklasz, S.D., and Garrow, T.A. (1997). Betaine-homocysteine methyltransferase expression in porcine and human tissues and chromosomal localization of the human gene. Arch. Biochem. Biophys. *345*, 171–174.

Takahashi, I., Yamada, Y., Kadowaki, H., Horikoshi, M., Kadowaki, T., Narita, T., Tsuchida, S., Noguchi, A., Koizumi, A., and Takahashi, T. (2010). Phenotypical variety of insulin resistance in a family with a novel mutation of the insulin receptor gene. Endocr. J. *57*, 509–516.

Tastekin, D., Erturk, K., Bozbey, H.U., Olmuscelik, O., Kiziltan, H., Tuna, S., and Tas, F. (2015). Plasma homocysteine, folate and vitamin B12 levels in patients with lung cancer. Exp. Oncol. *37*, 218–222.

Wandel, S., Schurmann, A., Becker, W., Summers, S.A., Shanahan, M.F., and Joost, H.G. (1995). Mutation of two conserved arginine residues in the glucose transporter GLUT4 supresses transport activity, but not glucose-inhibitable binding of inhibitory ligands. Naunyn Schmiedebergs Arch. Pharmacol. *353*, 36–41.

Wang, T.J., Larson, M.G., Vasan, R.S., Cheng, S., Rhee, E.P., McCabe, E., Lewis, G.D., Fox, C.S., Jacques, P.F., Fernandez, C., et al. (2011). Metabolite profiles and the risk of developing diabetes. Nat. Med. *17*, 448–453.

Wang, D., Wang, F., Shi, K.H., Tao, H., Li, Y., Zhao, R., Lu, H., Duan, W., Qiao, B., Zhao, S.M., et al. (2017). Lower Circulating Folate Induced by a Fidgetin Intronic Variant Is Associated With Reduced Congenital Heart Disease Susceptibility. Circulation *135*, 1733–1748.

Wang, D., Zhao, R., Qu, Y.Y., Mei, X.Y., Zhang, X., Zhou, Q., Li, Y., Yang, S.B., Zuo, Z.G., Chen, Y.M., et al. (2018). Colonic Lysine Homocysteinylation Induced by High-Fat Diet Suppresses DNA Damage Repair. Cell Rep. *25*, 398–412.e6.

Wilding, J.P. (2007). The importance of free fatty acids in the development of Type 2 diabetes. Diabet. Med. *24*, 934–945.

Yang, N., Yao, Z., Miao, L., Liu, J., Gao, X., Fan, H., Hu, Y., Zhang, H., Xu, Y., Qu, A., and Wang, G. (2015). Novel Clinical Evidence of an Association between Homocysteine and Insulin Resistance in Patients with Hypothyroidism or Subclinical Hypothyroidism. PLoS One *10*, e0125922.

Yilmaz, N., Pektas, M., Tonguc, E., Kilic, S., Gulerman, C., Gungor, T., and Mollamahmutoglu, L. (2008). The correlation of plasma homocysteine with insulin resistance in polycystic ovary syndrome. J. Obstet. Gynaecol. Res. *34*, 384–391.

Zhang, X., Xu, J., Cai, X., Ji, L., Li, J., Cao, B., Li, J., Hu, D., Li, Y., Wang, H., et al. (2014). Acute insulin resistance mediated by advanced glycation end-products in severely burned rats. Crit. Care Med. *42*, e472–e480.

Zhang, S.Y., Dong, Y.Q., Wang, P., Zhang, X., Yan, Y., Sun, L., Liu, B., Zhang, D., Zhang, H., Liu, H., et al. (2018). Adipocyte-derived Lysophosphatidylcholine Activates Adipocyte and Adipose Tissue Macrophage Nod-Like Receptor Protein 3 Inflammasomes Mediating Homocysteine-Induced Insulin Resistance. EBioMedicine *31*, 202–216.

Zhao, J.Y., Yang, X.Y., Gong, X.H., Gu, Z.Y., Duan, W.Y., Wang, J., Ye, Z.Z., Shen, H.B., Shi, K.H., Hou, J., et al. (2012). Functional variant in methionine synthase reductase intron-1 significantly increases the risk of congenital heart disease in the Han Chinese population. Circulation *125*, 482–490.

Zhao, J.Y., Yang, X.Y., Shi, K.H., Sun, S.N., Hou, J., Ye, Z.Z., Wang, J., Duan, W.Y., Qiao, B., Chen, Y.J., et al. (2013). A functional variant in the cystathionine β-synthase gene promoter significantly reduces congenital heart disease susceptibility in a Han Chinese population. Cell Res. *23*, 242–253.

Zhao, J.Y., Qiao, B., Duan, W.Y., Gong, X.H., Peng, Q.Q., Jiang, S.S., Lu, C.Q., Chen, Y.J., Shen, H.B., Huang, G.Y., et al. (2014). Genetic variants reducing MTR gene expression increase the risk of congenital heart disease in Han Chinese populations. Eur. Heart J. *35*, 733–742.

Zhu, H., Shyh-Chang, N., Segrè, A.V., Shinoda, G., Shah, S.P., Einhorn, W.S., Takeuchi, A., Engreitz, J.M., Hagan, J.P., Kharas, M.G., et al.; DIARAM Consortium; MAGIC Investigators (2011). The Lin28/let-7 axis regulates glucose metabolism. Cell *147*, 81–94.

STAR★METHODS

KEY RESOURCES TABLE

REAGENT or RESOURCE	SOURCE	IDENTIFIER
Antibodies		
phospho-Insulin Receptor β (T1150/1151)	Cell Signaling Technology	Cat# 3024; RRID: AB_331253
phospho-AS160(T642)	Cell Signaling Technology	Cat# 8881; RRID: AB_2651042
AS160	Cell Signaling Technology	Cat# 2670; RRID: AB_2199375
phospho-AKT(T308)	Cell Signaling Technology	Cat# 13038; RRID: AB_2629447
AKT2	Cell Signaling Technology	Cat# 3063; RRID: AB_2225186
Na-k-ATPase	Cell Signaling Technology	Cat# 23565S; RRID: AB_2798866
PDI	Cell Signaling Technology	Cat# 3501; RRID: AB_2156433
Insulin Receptor β	Cell Signaling Technology	Cat# 23413
Insulin Receptor α	Cell Signaling Technology	Cat# 74118; RRID: AB_2799850
Insulin	Cell Signaling Technology	Cat# 8138S; RRID: AB_10949314
FLAG	Abmart	Cat# M20008; RRID: AB_2713960
HA	Abmart	Cat# M20003
GAPDH	Sigma	Cat# G8795; RRID: AB_1078991
GM130	Abcam	Cat# ab52649
Calnexin	Proteintech	Cat# 10427-2-AP; RRID: AB_2069033
Actin	GenScript	Cat# A00702; RRID: AB_914102
Alexa Fluor 488 goat anti-mouse IgG	Invitrogen	Cat# A-11001; RRID: AB_2534069
Myc	Abmart	Cat# M20002
Furin	Abcam	Cat# ab3467; RRID: AB_303828
anti-mouse secondary antibodies	GenScript	Cat# A00160
anti-rabbit secondary antibodies	GenScript	Cat# A00098
Bacterial and virus strains		
BL21(DE3)	Vazyme	C504-02/03
AAV2/9-CMV_bGI-PDIA1-P2A-mCherry-SV40pA	Shanghai Taitool Bioscience	N/A
AAV2-CMV_bGI-PDIA1-MCS	Shanghai Taitool Bioscience	N/A
AAV2-hTBG-PDIA1-MCS	Shanghai Taitool Bioscience	N/A
AAV2-hAdp-PDIA1-MCS-EGFP-WPRE-SV40pA	Shanghai Taitool Bioscience	N/A
AAV2/9-CMV_bGI-INSR-P2A-mCherry-SV40pA	Shanghai Taitool Bioscience	N/A
Chemicals, peptides, and recombinant proteins		
Penicillin-Streptomycin	Invitrogen	Cat#15070063
DAPI	Sigma-Aldrich	Cat#D8417
DMEM, no glutamine	GIBCO	Cat#11960044
F-12 HAM'S(1X)	Hyclone	Cat#SH30026.01
sequencing grade modified trypsin	Promega	Cat#V5111
Anti-FLAG M2 Magnetic Beads	Sigma	Cat#M8823
TFA	Sigma	Cat#302031
synthetic peptides	GL Biochem	N/A
protein-A Sepharose bead	Merck Millipore	Cat#16-156
polyethylenimine (linear, 25 KDa)	Polysciences	Cat# 23966
ER-Tracker Red	Beyotime	Cat#C1041
Golgi-Tracker Red	Beyotime	Cat#C1043
L-Homocysteine	Sigma	Cat#69453

Continued

REAGENT or RESOURCE	SOURCE	IDENTIFIER
Critical commercial assays		
Glucose Uptake-Glo Assay	Promega	J1341
Endoplasmic Reticulum Isolation Kit	Sigma	ER0100
Plasma Membrane Protein Isolation Kit	Minute	SM-005
Total cholesterol (TC) ELISA kit	kanglang Biotech	KL-TC-Mu
Triglyceride (TG) ELISA kit	kanglang Biotech	KL-TG-Mu
High-density lipoprotein cholesterol (HDL-c) ELISA kit	kanglang Biotech	KL-HDL-c-Mu
Low-density lipoprotein cholesterol(LDL-c) ELISA kit	kanglang Biotech	KL-LDL-c-Mu
Insulin ELISA kit	kanglang Biotech	KL-INS-Mu
Homocysteine ELISA kit	kanglang Biotech	KL-Hcy-Mu
proinsulin ELISA kit	kanglang Biotech	KL-Proinsulin-Mu
C-peptide ELISA kit	kanglang Biotech	KL-CP-Mu
ClonExpress MultiS One Step Cloning Kit	Vazyme	Cat#C113-02
Experimental models: Cell lines		
HEK293T	ATCC	CRL-11268
CHO	ATCC	CCL-61
C2C12	ATCC	CRL-1772
HepG2	ATCC	HB-8065
HL-1	Procell	CL-0605
H9c2	ATCC	CRL-1446
LO2	Procell	CL-0111
Experimental models: Organisms/strains		
C57BL/6J	Beijing Vital River Laboratory Animal Technology Co. Ltd	N/A
Oligonucleotides		
Oligonucleotides are listed in Table S1	This study	N/A
Recombinant DNA		
Expression plasmid for IR	This study	N/A
Expression plasmid for Furin	This study	N/A
Expression plasmid for MARS	This study	N/A
Expression plasmid for PDIA1	This study	N/A
Software and algorithms		
ImageJ	NIH	https://imagej.nih.gov/ij/
GraphPad Prism 6	GraphPad Software	https://www.graphpad.com/scientific-software/prism/
MaxQuant	Matthias Man	http://www.coxdocs.org/doku.php?id=maxquant:start

RESOURCE AVAILABILITY

Lead contact
Further information and requests for resources and reagents should be directed to and will be fulfilled by the Lead Contact, Jian-Yuan Zhao (zhaojy@fudan.edu.cn).

Materials availability
All unique/stable reagents generated in this study will be made available upon request to the Lead Contact.

Data and code availability

- All data reported in this paper will be shared by the lead contact upon request.
- This study did not generate unique code.
- Any additional information required to reanalyze the data reported in this paper is available from the lead contact upon request.

EXPERIMENTAL MODEL AND SUBJECT DETAILS

Tissue cell lines

Human normal liver cell line (LO2), human liver cancer cell line (HepG2), mouse cardiac muscle cells (HL-1), mouse muscle cells (C2C12), and myogenic cells from embryonic rat heart ventricle (H9C2) were cultured in normal Dulbecco's modified Eagle's medium (DMEM; HyClone), supplemented with 10% fetal bovine serum (FBS), 100 units/mL penicillin (Invitrogen), and 100 mg/mL streptomycin (Invitrogen). Chinese hamster ovary cell line (CHO) were cultured in Ham's F-12 nutrient mixture (HyClone) supplemented with 10% fetal bovine serum (FBS), 100 units/mL penicillin (Invitrogen), and 100 mg/mL streptomycin (Invitrogen). All the cells were maintained at 37°C in a humidified 5% CO_2 atmosphere.

Mouse model

Six-week-old male C57BL/6J mice were obtained from Vital River (Beijing, China). The mice were maintained on a standard diet and had free access to water. For the experiment, the mice were housed in cages in a light-, temperature- and humidity-controlled environment. The wild-type mice were randomly divided into the control and high-Hcy groups. Vehicle or 2 g/L Hcy in water was orally administered *ad libitum* for 16 weeks. The food intake and water intake in control and high-Hcy groups were provided in Figures S4A and S4B. Blood glucose level was measured after 8−10 h of fasting every 4 weeks. Eight hours before animals were sacrificed, 2g/L Hcy water was replaced with normal water. Mice at 22 weeks of age were sacrificed to collect blood and tissues for the subsequent experiments. All animal experiments were approved by the Fudan University Animal Care and Use Committee and were conducted following the National Institutes of Health Guidelines for the Care and Use of Laboratory Animals.

For the construction of *PDI* overexpressing mice, the AAV2/9-CMV_bGI-PDIA1-P2A-mCherry-SV40pA (AAV2/9-PDI) virus was obtained from Shanghai Taitool Bioscience Co. Ltd. Recombinant AAV vectors (4×10^{11} V.G./mouse) were administered intravenously via the tail vein into mice. We next constructed tissue-specific *PDI* overexpressing mice models. For instance, to increase the PDI levels in muscle tissue, we injected the AAV-PDI virus with the CMV promoter (AAV2-CMV_bGI-PDIA1-MCS) locally. To overexpress PDI in the liver, we injected the AAV-PDI virus with a liver-specific promoter (AAV2-hTBG-PDIA1-MCS) through tail vein injection. The AAV-PDI virus with a fat-specific promoter (AAV2-hAdp-PDIA1-MCS-EGFP-WPRE-SV40pA) was injected locally to increase the PDI levels in adipose tissue. For the construction of *INSR* overexpressing mice, AAV2/9-CMV_bGI-INSR-P2A-mCherry-SV40pA (AAV2/9-INSR) virus was obtained from Shanghai Taitool Bioscience Co. Ltd. Recombinant AAV vectors (4×10^{11} V.G./mouse) were administered intravenously via the tail vein into mice.

METHOD DETAILS

Plasmid construction

The full-length sequences of human *INSR, PDI,* and *FURIN* open reading frames were obtained using polymerase chain reaction (PCR). The primer sequences were provided in Table S1. The PCR fragments were inserted into pcDNA3.1-FLAG, pcDNA3.1-Myc, or pCDNA3.1-HA vector using recombinant DNA technology and were confirmed via sequencing.

Cell transfections and co-immunoprecipitation

Plasmid transfections were carried out by the Polyethylenimine (PEI), Lipofectamine 3000 (Invitrogen), or Lipofectamine 2000 (Invitrogen) methods. In the PEI transfection method, 400 μL of DMEM (serum-free medium) and the plasmid were placed in an empty EP tube and PEI was added into the medium. The mixture was incubated for 15 min. Meanwhile, the cell culture medium was replaced with fresh 10% FBS medium. After 15 min, the mixture was added to the cells, and the fresh medium was replaced after 12 −16h. After 36-48 h, the transfection was completed. In the Lipofectamine 3000 transfection method. DMEM (250 μL) was added to two empty EP tubes and Lipofectamine 3000 was added to one of the tubes and mixed for 5 min. The plasmid and P3000 were added in the other tube and then added to the medium containing Lipofectamine 3000, mixed, and allowed to stand for 5 min. Meanwhile, the cell culture medium was replaced with fresh 10% FBS medium. After 5 min, the mixture was added to the cells, and the fresh medium was replaced after 12 h. After 36-48 h, the transfection was completed and the cells were treated. In the Lipofectamine 2000 transfection method, 125 μL of DMEM (serum-free medium) and the siRNA were placed in an empty EP tube. 125 μL of DMEM (serum-free medium) and the Lipofectamine 2000 were placed in another empty EP tube then added to the medium containing siRNA. The mixture was incubated for 5 min. Meanwhile, the cell culture medium was replaced with fresh 10% FBS medium. After 5 min, the mixture was added to the cells. After 36-48 h, the transfection was completed.

For immunoprecipitation, the cells were lysed with 0.5% NP-40 buffer containing 50 mM Tris-HCl (pH 7.5), 150 mM NaCl, 0.5% Nonidet P-40, 1 μg/mL aprotinin, 1 μg/mL leupeptin, 1 μg/mL pepstatin, and 1 mM phenylmethylsulfonyl fluoride (PMSF). Cell lysates were incubated with FLAG beads (Sigma) for 3 h at 4°C. The bound complexes were washed with 0.5% NP-40 buffer and mixed with loading buffer for analysis using sodium dodecyl sulfate-polyacrylamide gel electrophoresis (SDS-PAGE).

Reverse transcription and quantitative reverse transcription-PCR (qRT-PCR)

Total RNA was isolated from cultured cells and converted into cDNA using specific primers and the HiScript III cDNA synthesis kit (Vazyme, Nanjing, China). The mRNA levels of IR were determined using qRT-PCR with the CFX96 Touch real-time PCR detection system (Bio-Rad, Hercules, CA, USA). *GAPDH* or *ACTIN* was used as the internal reference gene. Each reaction was performed in triplicate. The primers used in this procedure are listed in the Table S1.

Western blotting

Cultured cells, and mouse tissues were lysed using 0.5% NP-40 buffer containing 50 mM Tris-HCl (pH 7.5), 150 mM NaCl, 0.5% Nonidet P-40, and a mixture of protease inhibitors (Sigma-Aldrich, St. Louis, Missouri, USA). After centrifugation at 16,000 × *g* and 4°C for 15 min, the lysate supernatants were analyzed via western blotting according to standard procedures. Protein abundance was detected by measuring chemiluminescence on a Typhoon FLA 9500 (GE Healthcare, Little Chalfont, UK).

Immunofluorescence

CHO cells were cultured overnight and transfected with IR-FLAG constructs using Lipofectamine 3000 per the manufacturer's protocol. When required, the transfected cells were treated with Hcy (2 mM), and probes for the Golgi body or the ER were added before fixation. Twenty-four hours post-transfection, the cells were washed with phosphate buffered saline (PBS, pH 7.4), fixed with 4% paraformaldehyde for 10 min, and washed in PBS thrice for 5 min each time. The cells were then permeabilized with 0.25% Triton X-100 in PBS for 5 min, washed thrice in PBS, and incubated in PBS containing 10% bovine serum albumin (BSA) for 1 h at room temperature to suppress non-specific binding of IgG. Then, the cells were washed with PBS and incubated with 1:500 dilution of the anti-FLAG antibody in PBS containing 3% BSA for 2 h at room temperature. Next, the cells were washed thrice with PBS for 5 min each time and incubated in PBS containing 3% BSA and Alexa Fluor 488-conjugated goat anti-mouse IgG for 1 hour at room temperature. Then, the cells were washed thrice with PBS for 5 min each time and incubated with 4′,6-diamidino-2-phenylin-dole (DAPI) for nuclear staining. The cells were observed under a fluorescence microscope (Olympus FV3000, Tokyo, Japan).

Glucose uptake

Glucose uptake assays were performed per the manufacturer's protocols (#J1341; Promega, Madison, Wisconsin, USA). The glucose uptake measurements were based on the detection of 2-deoxyglucose-6-phosphate (2DG-6P) using NADPHGlo technology, in which oxidation of 2DG-6P was coupled with NADPH production and its subsequent bioluminescent detection using a reductase/luciferase system. The cells were seeded at the density 10,000 cells/well in the 96-well plate and grown overnight. The, the cells were starved in DMEM without glucose for 2 h, followed by the addition of 1 mM 2DG solution. Glucose uptake was measured after 30 min. An inactivation solution was added to inactivate the endogenous glucose-6P-dehydrogenase (G6PDH) and to prevent NADPH destruction after 30 min. The measurement reagent consisted of luciferase buffer, GO buffer, NADP$^+$, G6PDH, reductase, and reductase substrate.

Drug affinity responsive target stability

HepG2 cells, transfected with IR-Flag, were plated on 6-well plates and the cells were lysed with M-PER buffer containing protease/phosphatase inhibitors on ice. Whole-cell lysates were diluted with 10 × TNC buffer [50 mM Tris-HCl (pH 8.0), 50 mM NaCl, 10 mM CaCl$_2$]. The cell lysates were treated with various concentrations (0, 1, and 2 mM) of homocysteine or cystathionine, or methionine for 1 h. Then, cell lysates were treated with pronase (1:100, 1:200, and 1:500 ratio) for 10 min at 37°C and the reaction was stopped by adding 0.5 M EDTA solution. The reaction mixtures were separated on a 10% SDS gel and identified using the Flag antibody at the size of pro-IR.

Surface plasmon resonance

The binding affinity of pro-IR with small molecules were analyzed by SPR (Biacore T200, GE Healthcare). The purified 5mg/ml pro-IR protein was covalently immobilized to a CM5 sensor chip through amine group in 10 mM sodium acetate buffer (pH 5.5). Small molecules were diluted to 100 μM solutions. The procedure was performed following the manufacturer's instructions.

PDI purification

To obtain recombinant PDI, the PDI coding region was amplified using PCR with specific primers showed in Table S1. The PCR product was inserted into the pET-28az (+) vector. The expression plasmid, pET-28a-sPDI, was used to transform *Escherichia coli* BL21 (DE3) strains [genotype: F$^-$ ompT hsdS (r$_B^-$ m$_B^-$) gal dcm (DE3)] and positive clones were selected on Luria Bertani (LB)/kanamycin plates at 37°C with vigorous shaking. *Escherichia coli* BL21 (DE3) strains were cultured in Luria Bertani (LB) (10 g trypone, 5g yeast extract and 10 g NaCl in 1L dH$_2$O, pH 7.4) with 50 mg/L kanamycin at 37°C. Isopropyl β-D-1-thiogalactopyranoside (IPTG) was added

to a final concentration of 0.5 mM when the OD_{600} of the culture reached 0.6–0.8. The cultures were incubated for 12 more hours at 18°C after which they were harvested via centrifugation. The harvested cells were re-suspended in 50 mM Tris–HCl, 500 mM NaCl, and 20 mM imidazole (pH 7.0) and sonicated on ice for 99 cycles with 4 s working and 4 s intermission. The cell lysate was centrifuged at 13,663 × g for 30 min at 4°C. The supernatant of the total cell extract was loaded onto a Ni^{2+}-chelating Sepharose Fast Flow column (GE Healthcare), which was charged with Ni^{2+} ions and preequilibrated with lysis buffer. The column was exhaustively washed with the lysis buffer until the absorbance value at 280 nm reached the baseline. The recombinant protein was eluted via three step-elution with a series of elution buffers (50 mM Tris–HCl, pH 7.0, and 500 mM NaCl with 100 mM, 200 mM and 350 mM imidazole). All the elution fractions were collected and analyzed using SDS-PAGE. Fractions containing the fusion protein were applied to a Sephadex G-25 fine column (GE Healthcare), and the buffer was exchanged with PBS for further functional studies.

In vitro modification
In vitro reactions were performed in a 30 μL reaction volume containing 50 mM Tris-HCl (pH 8.0), 3 mM Hcy, 1 mM PMSF, and 0.05 mg/mL synthetic substrate peptide. The reaction was allowed to continue for 12 h at 37°C. The peptide was desalted by passing through a C18 ZipTip (Millipore, Billerica, MA, USA) and then analyzed using a matrix-assisted laser desorption ionization-time of flight (MALDI-TOF)/TOF mass spectrometer (SCIEX-5800, Framingham, Massachusetts, USA).

In vitro de-modification
In vitro de-modification reactions were performed in a 30 μL reaction containing 100 mM K_3PO_4 (pH 7.5), 2 mM EDTA, 0.3 mM di-thiothreitol (DTT), 0.05 mg/mL synthetic aminoacylated peptide, 0.2 mg/mL PDI, and 1 mM PMSF. The reaction was allowed continue for 30 min at 37°C. The peptide was desalted by passing through a C18 ZipTip (Millipore, Billerica, MA, USA) and analyzed using a MALDI-TOF/TOF mass spectrometer (SCIEX-5800).

Sample preparation and liquid chromatography-tandem mass spectrometry (LC-MS)/MS analysis
To identify C-Hcy sites on target proteins, HepG2 cells were transfected with pcDNA3.1-Flag-IR and treated with Hcy (2 mM, 10 h). After the cells were harvested, supernatants containing FLAG-bound beads were collected and digested with trypsin at a trypsin: protein ratio of 1:50. The obtained peptides were stored at 80°C until analysis using LC-MS/MS. LC-MS/MS was performed on an EASY-nLC100 (Thermo Scientific) coupled with Orbitrap Elite (Thermo Scientific) and equipped with an online nano-electrospray ion source. The obtained peptides were desalted and suspended in 10 μL solvent A (A: water with 0.1% formic acid; B: ACN with 0.1% formic acid). Each sample was loaded onto a self-packed C18 column (100 μm × 2 cm, 5-μm particle size) at a flow rate of 5 μL/min for 5 min, and subsequently separated on an analytical column (C18, 75 μm × 20 cm) with a linear gradient from 5% B to 90% B over 120 min. The column was re-equilibrated under initial conditions for 15 min. The column flow rate was maintained at 200 nL/min. The mass spectrometer was set as follows: ion-transfer capillary, 275°C; spray voltage, 2 kV; full MS range, 400–2,000 m/z. Full mass spectra were acquired at a resolution of 60,000, with a target ion setting of 10^6. One full MS scan was followed by 15 MS/MS scans, and multistage activation was enabled. The dynamic exclusion function was set as follows: repeat count, 2; repeat duration, 30 s; exclusion duration, 60 s.

For quantification of targeted homocysteinylated peptides, briefly, a ratio of homocysteinylated peptide signal [the total ion counts (TIC) of homocysteinylated form (TIC_{C-Hcy})] to the total peptide signal [TIC_{C-Hcy} + TIC of the non-homocysteinylated form ($TIC_{non-C-Hcy}$] were calculated using the following equation: Ratio of C-Hcy (R_{C-Hcy}) = $TIC_{C-Hcy}/(TIC_{C-Hcy}+TIC_{non-C-Hcy})$.

C-Hcy site identification
Raw MS files were analyzed using MaxQuant version 1.4.1.2. The MS/MS spectra were searched using the Andromeda search engine against the SwissProt-human database (Release 2014-04-10) containing forward and reverse sequences. In the main Andromeda search precursor, mass and fragment mass had an initial mass tolerance of 5 ppm and 0.05 Da, respectively. The search included homocysteinylation of cysteine, protein N-acetylation, and oxidation of methionine. Minimal peptide length was set to seven amino acids, and a maximum of four miscleavages was allowed. The false discovery rate (FDR) was set to 0.01 for peptide and protein identification.

Cellular fractionation
Membrane was isolated from cells using a plasma membrane protein isolation kit (Minute, SM-005). Microsomes (endoplasmic reticulum and the Golgi) apparatus were isolated from cells using an endoplasmic reticulum isolation kit (Sigma, ER0100).

Insulin and glucose tolerance tests
ITT (2 IU/kg insulin i.p.) and GTT (2 g/kg glucose i.p.) were performed in mice (8 weeks after vehicle or Hcy treatment) after 6 h of fasting. For ITT, blood glucose level was assessed 0, 15, 30, 60, and 120 min after injection using a glucose meter (Roche, Accu-chek). Data were expressed as blood glucose change relative to that at 0 min. For GTT, blood glucose level was assessed at 0, 15, 30, 60, and 120 min after the injection using a glucose meter; absolute data are showed.

Plasma insulin, proinsulin, and C-peptide detection

The levels of fasting proinsulin and C-peptide of mice in control and Hcy-treated groups were detected using ELISA (Kanglang Biotech, Shanghai, China). Fasting insulin level in the plasma was determined using the insulin ELISA kit per the manufacturer's instructions (Kanglang Biotech) and western blotting. The ELISA signal was read at 450 nm using a microplate reader (iMark, BIORAD, Hercules, CA, USA). For western blotting, albumin was considered as the reference protein.

Hcy quantification

To obtain plasma from mice, one eyeball from each animal was ejected with scissors and completely removed. Blood from the retro-orbital plexus was collected in EDTA-coated 1.5 mL tubes and centrifuged immediately. Then, the plasma samples were collected and stored at $-80°C$ until determination of Hcy content using a homocysteine ELISA kit (Kanglang Biotech).

QUANTIFICATION AND STATISTICAL ANALYSIS

Differences between groups were examined using one-way analysis of variance (ANOVA) when appropriate, with the Bonferroni post hoc test. All p values below 0.05 were considered significant. Data are presented as mean $\pm$ SD. For GTT and ITT, two-way ANOVA with multiple comparisons were performed for statistical analyses. Additionally, the area under curve (AUC) of each mouse was calculated and further evaluated by a two-tailed unpaired t test with/without Welch's correction or one-way ANOVA. Sample size and specific statistical tests used in experiments are shown in the figure legends.